Three-Dimensional Analysis of Ice Sheet Indentation: Limit Analysis Solutions

D. G. Karr

J. C. Watson

M. HooFatt

Department of Ocean Engineering,
Massachusetts Institute of Technology,
Cambridge, MA 02139

A method is presented for determining the collapse pressures of an ice sheet subjected to a uniformly distributed edge load by applying the upper-bound theorem of limit analysis. The ice sheet is idealized as a semi-infinite layer of elastic-perfectly plastic material. A quadratic anisotropic yield criterion is used to calculate the indentation pressures. The ice sheet consists of columnar ice and is assumed isotropic in the plane of the ice sheet. Upper-bound solutions are found by optimizing a three-dimensional discontinuous velocity field representing an assumed collapse pattern of the ice sheet. Solutions are based on various ratios of indentor width to ice thickness, thereby providing an envelope of indentation pressures over a range of aspect ratios, from conditions of plane strain to plane stress. Solutions are then compared with corresponding two and three-dimensional lower-bound analyses.

I Introduction

A fundamental problem in the design of fixed structures for offshore Arctic service is that of predicting the force an ice sheet exerts on a structure as it is driven against the structure by environmental forces. Quantifying structural loads due to ice impact depends to a great extent on a knowledge of how the ice sheet fails. The problem is complicated by the fact that ice is a rate-dependent material which may exhibit both ductile and brittle behavior during the ice sheet indentation process. In addition, the geometry of the problem requires an understanding of the mechanical properties of ice under multi-axial states of stress. Temperature and material characteristics such as grain size and structure, salinity, porosity and natural imperfections are also important factors.

The layout of the ice sheet indentation problem is shown in Fig. 1. A rectangular structure of width D is assumed to be in perfect contact with the flat, leading edge of a moving ice sheet of thickness t and with velocity V. The manner in which the ice sheet fails is thought to be governed by the nominal strain rate and by the aspect ratio, defined by the ratios V/D (or V/t) and D/t, respectively.

The influence of strain rate and aspect ratio on the ice-structure interaction process has been addressed in a number of studies (Bohon and Weingarten, 1985; Palmer et al., 1983; Timco, 1986; Michel and Toussaint, 1977; Ralston, 1978; Reinicke and Remer, 1978; Croasdale, Morgenstern and Nuttal, 1977). At high rates of strain, ice behaves as a brittle material and failure is dominated by cracking and fracture. At low strain rates ice exhibits ductile behavior characterized by creep and continuous crushing deformation. The aspect ratio defines the general state of stress in the proximity of the ice-structure contact. Large aspect ratios correspond to the conditions of plane stress in which transverse stresses vanish for thin plates subject to in-plane loads. Small aspect ratios reflect the conditions of plane strain in which transverse, out-of-plane strains are assumed to vanish. Problems of plane stress and plane strain are often reduced to two-dimensional analyses. Between these extremes of aspect ratios and strain rates, ice sheet indentation involves a three-dimensional stress field and mix of deformation modes.

In this study, ice is treated as a plastically deforming continuum, whereby failure or collapse of the ice sheet takes place at constant stress. The load required to initiate indentation can then be determined using the theorems of limit analysis. Although the cracking and fracture phenomena observed in ice sheet indentation are ignored in this type of analysis, the three-dimensional nature of the problem at intermediate values of the aspect ratio can be addressed. Solutions based on plasticity theory can also provide insights for other approaches to the problem (Wierzbicki and Karr, 1987; Sanderson, 1986).

II Plasticity and Limit Analysis

Limit analysis is concerned with the determination of the loads which will cause collapse of a body (Chen, 1975). In this respect, limit analysis is well suited to the ice sheet indentation problem, since the load at which the ice sheet fails is the force imparted to the structure. The theorems of limit analysis are based on the concept of perfect plasticity. While the assumption of perfectly plastic material behavior at failure may be an appropriate idealization for the ice sheet indentation problem at low strain rates, it represents a limitation to the solution of the problem at high strain rates in which brittle, discontinuous failure modes may be involved.

In order to apply the theorems of limit analysis, the point

Contributed by the OMAE Division and presented at the 6th International Symposium and Exhibit on Offshore Mechanics and Arctic Engineering, Houston, Texas, March 1–5, 1987, of THE AMERICAN SOCIETY OF MECHANICAL ENGINEERS. Manuscript received by the OMAE Division, 1987; revised manuscript received October 7, 1988.

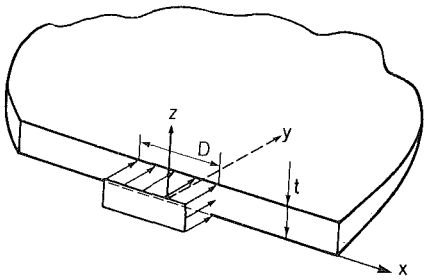

Fig. 1 Indentation geometry for a semi-infinite ice sheet

of transition from elastic to perfectly plastic material behavior must be defined. The transition occurs at the yield value and is defined mathematically by a yield function

$$F(\sigma_{ij}) = 0 \tag{1}$$

Yielding or plastic flow occurs when the stress intensity lies on the surface in stress space defined by $F = 0$. Stress states for $F > 0$ are not feasible for a perfectly plastic material (Drucker and Prager, 1952). The rate of plastic strain at yield is related to stress through the concept of a plastic potential, which is expressed as

$$\epsilon'_{ij} = \lambda \frac{\partial F}{\partial \sigma_{ij}} \tag{2}$$

where ϵ'_{ij} is the plastic strain rate component and λ is a positive, scalar proportionality factor. From a geometrical standpoint, equation (2) shows that the plastic strain rate vector, ϵ', has the direction of an outward-pointing normal to the yield surface described by F.

In summary, the methods of limit analysis require the following:

1 At the limit load, material behavior is perfectly plastic such that deformation proceeds at constant stress.

2 The yield function, which defines the transition from elastic to plastic material behavior, describes a convex surface in stress space and provides a means to calculate plastic strain rates through the concept of a plastic potential.

3 At the instant of collapse, changes in geometry of the body are negligible and therefore elastic strains can be ignored.

With these assumptions, the upper-bound theorem of limit analysis is stated as follows (Drucker and Prager, 1952):

> Collapse must occur if for any compatible flow pattern, considered as plastic only, the rate at which the external forces do work on the body equals or exceeds the rate of internal dissipation.

The rate of energy dissipation per unit volume is

$$D_v = \sigma_{ij}\epsilon'_{ij} \tag{3}$$

In this paper, a method is presented for determining three-dimensional, upper-bound solutions for edge-loaded semi-infinite ice sheets. This method, together with the procedures developed for lower-bound solutions (Karr, 1988), provide a means to bracket the load which will cause the body to collapse. In the lower-bound method, the approach is based on an analysis of stress distribution. In an upper-bound solution, the kinematics of failure deformations are addressed in which the rate of internal energy dissipation is calculated. These two features of the analysis are important, not only in assessing the accuracy of the solution, but also in gaining insight into the problem from two distinct viewpoints.

Discontinuous Velocity Fields. In the upper-bound solutions, collapse mechanisms may be represented by rigid body sliding patterns developed by segmenting the ice sheet into a number of blocks. Plastic deformation of the ice sheet results in relative motion between adjacent blocks, and therefore involves surfaces of velocity discontinuity within the sheet. The velocity discontinuity can be considered to be achieved through a transition layer of thickness, t, across which the velocity changes linearly from the magnitude on one side to that of another. The orientation of the surface of velocity discontinuity is defined by the unit normal vector, n.

The relations between plastic strain rate and the relative velocity and normal components for rigid body sliding were extended to three dimensions by Reinicke and Ralston (1977)

$$\epsilon'_{ij} = \frac{1}{2t}\left[n_j v_i + n_i v_j\right] \tag{4}$$

Thus, from an assumed velocity field, the strain rate components can be determined. The rate of energy dissipation, D_v, can then be determined from equation (3). The rate of energy dissipation per unit area of a surface of velocity discontinuity, D_A, is obtained by multiplying D_v by the thickness of the uniform transition layer, t, and taking the limit as the thickness goes to zero

$$D_A = \lim_{t\to 0}(tD_v) \tag{5}$$

Figure 2 shows a plane strain collapse mechanism consisting of three rigid blocks. Each block is prescribed a velocity V_1, V_2 and V_3, respectively, from which the relative velocities across the surface of discontinuity can be determined. The resulting rate of energy dissipation for the mechanism can then be calculated and the upper-bound theorem applied. For this case there are no vertical surface normal components and no vertical velocity components. The in-plane geometry shown in the figure is defined by the width of the indentor and five angles θ_1, θ_2, θ_3, θ_4 and θ_5.

This plane strain discontinuous velocity field is also shown in three dimensions in Fig. 3. We introduce in Fig. 3 two additional dependent angles θ_6 and θ_7 ($\theta_5 + \theta_7 = \theta_4 + \theta_6 = \pi/2$). Note that for the three-dimensional case, the angles θ_i are defined at the bottom of the ice sheet for which $z = 0$. The points A, B, C, D and E have the cartesian coordinates:

A (0, 0, 0) B (BLX, BLY, 0)

C (CLX, CLY, 0) D (DLX, 0, 0)

E (ELX, 0, 0)

where ELX is the width of the indentor and the remaining distances can be determined using the angles θ_i.

For a general three-dimensional analysis, vertical components of the surface normals and velocities are necessary. We therefore rotate the previously defined surfaces about their respective bottom edges. The line AB is rotated through an angle β_1, the line BC through an angle β_2, the line CD through an angle β_3, the line BE through an angle β_4, and the line CE through an angle β_5.

An example configuration of the rigid blocks is shown in

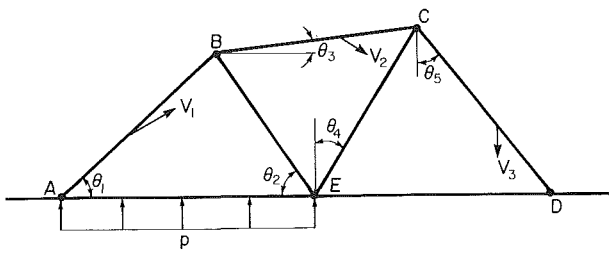

Fig. 2 Plane strain velocity field

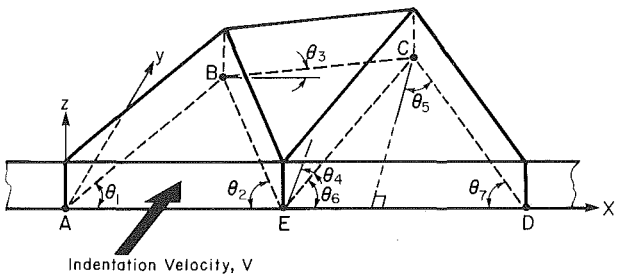

Fig. 3 Three-dimensional velocity field for plane strain

Fig. 4. Note that when surfaces intersect, various configurations may result, for example as shown in Fig. 5; the actual configuration depends on the relative values of the variables β_1, β_2, β_3, β_4 and β_5. For each case, however, the surfaced areas can be calculated by considering the positions of the intersection points, given as follows:

$$A_5 \quad \left(0,\ t\frac{\tan\beta_1}{\cos\theta_1},\ t\right)$$

$$A_6 \quad (0,\ 0,\ t)$$

$$B_4 \quad \left(BLX + \frac{t(\tan\beta_2\cos\theta_1 - \tan\beta_1\cos\theta_3)}{\cos\theta_1\cos\theta_3(\tan\theta_1 - \tan\theta_3)},\right.$$

$$\left. BLY + \frac{t(\tan\beta_2\sin\theta_1 - \tan\beta_1\sin\theta_3)}{\cos\theta_1\cos\theta_3(\tan\theta_1 - \tan\theta_3)},\ t\right)$$

$$B_5 \quad \left(BLX + \frac{t(\tan\beta_4\cos\theta_3 - \tan\beta_2\cos\theta_2)}{\cos\theta_2\cos\theta_3(\tan\theta_2 + \tan\theta_3)},\right.$$

$$\left. BLY + \frac{t(\tan\beta_2\sin\theta_2 + \tan\beta_4\sin\theta_3)}{\cos\theta_2\cos\theta_3(\tan\theta_2 + \tan\theta_3)},\ t\right)$$

$$B_6 \quad \left(BLX + \frac{t(\tan\beta_4\cos\theta_1 - \tan\beta_1\cos\theta_2)}{\cos\theta_1\cos\theta_2(\tan\theta_1 - \tan\theta_2)},\right.$$

$$\left. BLY + \frac{t(\tan\beta_4\sin\theta_1 - \tan\beta_1\sin\theta_2)}{\cos\theta_1\cos\theta_2(\tan\theta_1 + \tan\theta_2)},\ t\right)$$

$$C_4 \quad \left(CLX + \frac{t(\tan\beta_3\cos\theta_3 - \tan\beta_2\cos\theta_7)}{\cos\theta_7\cos\theta_3(\tan\theta_3 + \tan\theta_7)},\right.$$

$$\left. CLY + \frac{t(\tan\beta_3\sin\theta_3 + \tan\beta_2\sin\theta_7)}{\cos\theta_7\cos\theta_3(\tan\theta_3 + \tan\theta_7)},\ t\right)$$

$$C_5 \quad \left(CLX + \frac{t(\tan\beta_3\cos\theta_6 + \tan\beta_5\cos\theta_7)}{\cos\theta_7\cos\theta_6(\tan\theta_6 + \tan\theta_7)},\right.$$

$$\left. CLY + \frac{t(\tan\beta_3\sin\theta_6 - \tan\beta_5\sin\theta_7)}{\cos\theta_6\cos\theta_7(\tan\theta_6 + \tan\theta_7)},\ t\right)$$

$$C_6 \quad \left(CLX + \frac{t\tan\beta_5\cos\theta_3 + \tan\beta_2\cos\theta_6)}{\cos\theta_3\cos\theta_6(\tan a\,\theta_6 - \tan\theta_3)},\right.$$

$$\left. CLY + \frac{t(\tan\beta_2\sin\theta_6 + \tan\beta_5\sin\theta_3)}{\cos\theta_3\cos\theta_6(\tan\theta_6 - \tan\theta_3)},\ t\right)$$

$$D_2 \quad \left(DLX + t\frac{\tan\beta_3}{\cos\theta_5},\ 0,\ t\right)$$

$$E_2 \quad \left(ELX + t\frac{\tan\beta_4}{\sin\theta_2},\ 0,\ t\right)$$

$$E_3 \quad \left(ELX + t\frac{\tan\beta_5}{\cos\theta_4},\ 0,\ t\right)$$

Again, the three rigid blocks are assigned velocities V_1, V_2, and V_3. For the velocity profile shown in Fig. 4, there are nine surfaces of velocity discontinuity having relative velocities acting across surfaces defined in Table 1.

III Anisotropic Yield Function

A recently developed anisotropic failure criterion has been proposed to describe the failure envelope for sea ice (Karr et al., 1988). This anisotropic criterion is based on the generalized distortion energy (Olszak and Urbanowski, 1956) reaching a limiting value which is asymptotically dependent on the effective hydrostatic stress. Unlike many yield functions, this criterion is capable of predicting failure due to purely hydrostatic compression. A linearized approximation of this criterion was shown to describe the failure envelope of sea ice in a similar manner. This criterion is often referred to as the quadratic yield function (Tsai and Wu, 1971), and for orthotropic materials takes the form

$$\begin{aligned} F(\sigma_{ij}) = {} & a_1\sigma_{11}^2 + a_2\sigma_{22}^2 + a_3\sigma_{33}^2 \\ & + a_4\sigma_{22}\sigma_{33} + a_5\sigma_{33}\sigma_{11} + a_6\sigma_{11}\sigma_{22} \\ & + a_7\sigma_{23}^2 + a_8\sigma_{31}^2 + a_9\sigma_{12}^2 \\ & + a_{10}\sigma_{11} + a_{11}\sigma_{22} + a_{12}\sigma_{33} - 1 = 0 \end{aligned} \qquad (6)$$

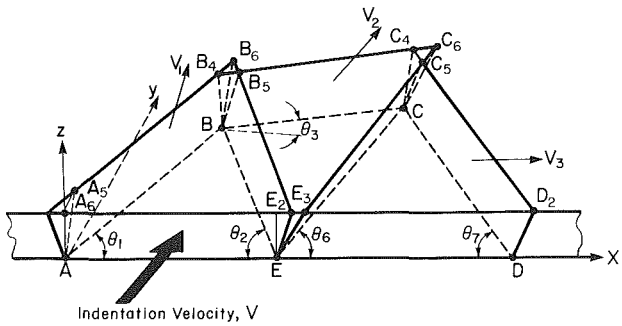

Fig. 4 An example three-dimensional velocity field geometry

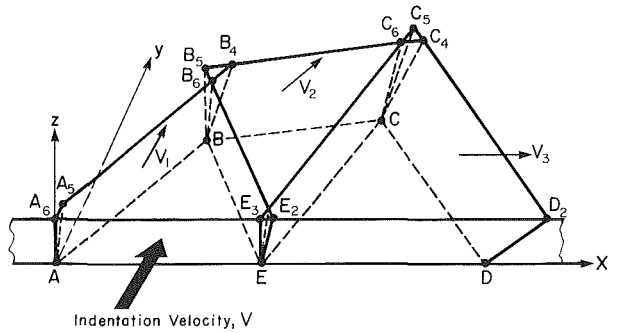

Fig. 5 Alternative three-dimensional velocity field geometry

Table 1 Discontinuous velocity field geometry

Area	Relative velocity	Surface area	Surface normals n_x	n_y	n_z
1	V_1	AA_5B_4B	$\sin\theta_1\cos\beta_1$	$-\cos\theta_1\cos\beta_1$	$\sin\beta_1$
2	V_2	BB_5CC_4	$\cos\beta_2\sin\theta_3$	$-\cos\beta_2\cos\theta_3$	$\sin\beta_2$
3	V_3	CC_5DD_2	$-\cos\theta_5\cos\beta_3$	$-\sin\theta_5\cos\beta_3$	$\sin\beta_3$
4	$V_2 - V_1$	BB_5EE_2	$\sin\theta_2\cos\beta_4$	$\cos\theta_2\cos\beta_4$	$-\sin\beta_4$
5	$V_3 - V_2$	CC_5EE_3	$\cos\theta_4\cos\beta_5$	$-\sin\theta_4\cos\beta_5$	$-\sin\beta_5$
6	V_1	AA_5A_6	1	0	0
7	V_1	BB_4B_5	$\cos\beta_2\sin\theta_3$	$-\cos\beta_2\cos\theta_3$	$\sin\beta_2$
8	V_2	CC_4C_5	$-\cos\theta_5\cos\beta_3$	$-\sin\theta_5\cos\beta_3$	$\sin\beta_3$

As sea ice is formed in nature, the c-axis of the hexagonal ice crystals tends to form in the horizontal plane of the ice sheet. This preferred orientation of the c-axis results in anisotropic strength characteristics of sea ice sheets. The strength properties are often isotropic within the plane of the ice sheet due to the random orientation of the c-axis in the horizontal plane. Designating the plane of the ice sheet as the $x_1 - x_2$ plane then, equation (6) is subject to the restrictions

$$a_1 = a_2, \qquad a_4 = a_5, \qquad a_7 = a_8,$$

and

$$a_9 = 2a_1 - a_6, \qquad a_{10} = a_{11}$$

Thus, for in-plane isotropy, equation (6) reduces to

$$\begin{aligned} F = {} & a_1(\sigma_{11}^2 + \sigma_{22}^2) + a_3\sigma_{33}^2 \\ & + a_4(\sigma_{22}\sigma_{33} + \sigma_{33}\sigma_{11}) + a_6\sigma_{11}\sigma_{22} \\ & + (2a_1 - a_6)\sigma_{12}^2 + a_8(\sigma_{23}^2 + \sigma_{31}^2) \\ & + a_{10}(\sigma_{11} + \sigma_{22}) + a_{12}\sigma_{33} - 1 = 0 \end{aligned} \tag{7}$$

A close fit to the multi-axial test results provided by Hausler (1981) can be achieved by using the following material coefficients:

$$\begin{aligned} a_1 &= 0.971 \text{ MPa}^{-2} & a_3 &= 0.100 \text{ MPa}^{-2} \\ a_4 &= -0.076 \text{ MPa}^{-2} & a_6 &= -1.61 \text{ MPa}^{-2} \\ a_8 &= 3.55 \text{ MPa}^{-2} & a_{10} &= 1.51 \text{ MPa}^{-1} \\ a_{12} &= 0.900 \text{ MPa}^{-1} \end{aligned} \tag{8}$$

The yield function given by equation (7) is not necessarily convex for arbitrary values of the coefficients. However, the use of the coefficients in equation (8) does result in a convex function. This was shown by Karr et al. (1988) using the convexity conditions described by Feng and Yang (1984). A description of the failure envelope using equations (7) and (8) is also provided.

An additional important feature of the quadratic yield function, when used with the associated flow rule, is the laterally confined compression strength. This is defined as the compressive value for σ_x when $\epsilon_y' = \epsilon_{xy}' = \epsilon_{zy} = \sigma_z = 0$. As shown in Fig. 6, the compressive strength in this case is $\sigma_x = -9.64$ MPa. In the following, it is shown that the ice sheet indentation strength is less than this value for high aspect ratios.

Rate of Dissipation of Energy. As shown by Karr et al. (1988), by application of equation (2), the stress, strain-rate relations are given by

$$\begin{aligned} \epsilon_{11}' &= \lambda(2a_1\sigma_{11} + a_5\sigma_{33} + a_6\sigma_{22} + a_{10}) \\ \epsilon_{22}' &= \lambda(2a_2\sigma_{22} + a_4\sigma_{33} + a_6\sigma_{11} + a_{11}) \\ \epsilon_{33}' &= \lambda(2a_3\sigma_{33} + a_4\sigma_{22} + a_5\sigma_{11} + a_{12}) \\ \epsilon_{23}' &= \lambda a_7\sigma_{23} \qquad \epsilon_{31}' = \lambda a_8\sigma_{31} \\ \epsilon_{12}' &= \lambda a_9\sigma_{12} \end{aligned} \tag{9}$$

Additionally, the rate of energy dissipation per unit volume is shown to be

$$\begin{aligned} D_v = {} & \lambda\left(2 + \frac{\bar{b}}{b}\right) - \frac{1}{b}[\epsilon_{11}'(b_1a_{10} + b_6a_{11} + b_5a_{12}) \\ & + \epsilon_{22}'(b_6a_{10} + b_2a_{11} + b_4a_{12}) \\ & + \epsilon_{33}'(b_5a_{10} + b_4a_{11} + b_3a_{12})] \end{aligned} \tag{10}$$

where

$$\begin{aligned} \lambda = \Bigg\{ \frac{1}{(2b + \bar{b})} \Bigg[& b_1\epsilon_{11}'^2 + b_2\epsilon_{22}'^2 + b_3\epsilon_{33}'^2 \\ & 2b_4\epsilon_{22}'\epsilon_{33}' + 2b_5\epsilon_{33}'\epsilon_{11}' + 2b_6\epsilon_{11}'\epsilon_{22}' \\ & + 2b\left(\frac{\epsilon_{23}'^2}{a_7} + \frac{\epsilon_{13}'^2}{a_8} + \frac{\epsilon_{12}'^2}{a_9}\right)\Bigg]\Bigg\}^{1/2} \end{aligned} \tag{11}$$

In addition,

$$\begin{aligned} b &= 8a_1a_2a_3 + 2a_4a_5a_6 \\ &\quad - 2(a_1a_4^2 + a_2a_5^2 + a_3a_6^2) \\ b_1 &= 4a_2a_3 - a_4^2 \\ b_2 &= 4a_1a_3 - a_5^2 \\ b_3 &= 4a_1a_2 - a_6^2 \\ b_4 &= a_5a_6 - 2a_1a_4 \\ b_5 &= a_4a_6 - 2a_2a_5 \\ b_6 &= a_4a_5 - 2a_3a_6 \end{aligned}$$

and

$$\bar{b} = b_1a_{10}^2 + b_2a_{11}^2 + b_3a_{12}^2 + 2(b_4a_{11}a_{12} + b_5a_{10}a_{12} + b_6a_{10}a_{11})$$

For the velocity fields to be kinematically admissible, the corresponding strain rates using equation (4) must be normal to the yield surface. We therefore seek to prove that an arbitrary strain rate field, $\bar{\epsilon}_{ij}'$, satisfies the normality condition and the yield function. Given $\bar{\epsilon}_{ij}'$, we may define an associated stress field, $\bar{\sigma}_{ij}$, which satisfies the normality requirement by inverting equations (9)

$$\bar{\sigma}_{11} = \frac{1}{b\lambda}[(b_1\bar{\epsilon}_{11}' + b_6\bar{\epsilon}_{22}' + b_5\bar{\epsilon}_{33}') - \lambda(b_1a_{10} + b_6a_{11} + b_5a_{12})]$$

$$\bar{\sigma}_{22} = \frac{1}{b\lambda}[(b_6\bar{\epsilon}_{11}' + b_2\bar{\epsilon}_{22}' + b_4\bar{\epsilon}_{33}') - \lambda(b_6a_{10} + b_2a_{11} + b_4a_{12})]$$

$$\bar{\sigma}_{33} = \frac{1}{b\lambda}[(b_5\bar{\epsilon}_{11}' + b_4\bar{\epsilon}_{22}' + b_3\bar{\epsilon}_{33}') - \lambda(b_5a_{10} + b_4a_{11} + b_3a_{12})]$$

$$\bar{\sigma}_{23} = \frac{\bar{\epsilon}_{23}'}{a_7\lambda} \qquad \bar{\sigma}_{31} = \frac{\bar{\epsilon}_{31}'}{a_8\lambda} \qquad \bar{\sigma}_{12} = \frac{\bar{\epsilon}_{12}'}{a_9\lambda} \tag{12}$$

Substituting equations (12) into the yield function results in an expression for λ in the form of equation (11), with ϵ_{ij}' replaced by $\bar{\epsilon}_{ij}'$. Thus, the normality condition and the yield function are satisfied provided λ is positive.

In order to show that λ is indeed positive for the particular values of the coefficients of equation (8), we note that the quantity $(2b + \bar{b})$ is positive. Furthermore, the coefficients b, a_7, a_8 and a_9 are also positive. Hence, λ is positive provided

$$\begin{aligned} & b_1\epsilon_{11}'^2 + b_2\epsilon_{22}'^2 + b_3\epsilon_{33}'^2 \\ & \quad + 2b_4\epsilon_{22}'\epsilon_{33}' + 2b_5\epsilon_{33}'\epsilon_{11}' + 2b_6\epsilon_{11}'\epsilon_{22}' > 0 \end{aligned} \tag{13}$$

Using the conditions described by Feng and Yang (1984), the left-hand side of equation (13) is positive semi-definite if

$$\begin{aligned} b_1 &\geq 0 & b_2 &\geq 0 & b_3 &\geq 0 \\ b_1b_2 - b_6^2 &\geq 0 & b_2b_3 - b_4^2 &\geq 0 \\ b_3b_1 - b_5^2 &\geq 0 \end{aligned} \tag{14}$$

Use of the coefficients of equation (8) satisfies all of the foregoing inequalities, and thus the normality condition is met and the yield function is satisfied for arbitrary strain rates.

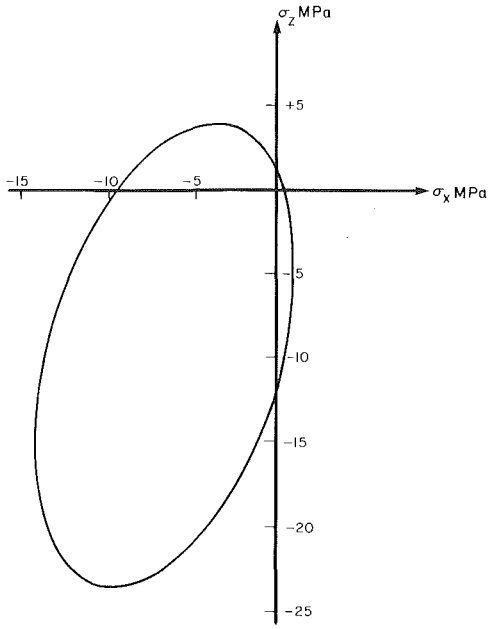

Fig. 6 Plane strain yield envelope in the $\sigma_x - \sigma_z$ plane ($\epsilon_y' = 0$)

IV Limit Analysis Solutions

Referring again to Fig. 4, for a particular thickness and indentation width, the geometry of the collapse mechanism is defined by the angles θ_i and β_i, $i = 1, 2, \ldots, 5$. The velocity field is defined by the components of V_1, V_2 and V_3 given by v_{1x}, v_{1y}, v_{1z}, v_{2x}, v_{2y}, v_{2z}, v_{3x}, v_{3y} and v_{3z}. Note that for the velocity profile to be kinematically admissable, the y component of block 1, v_{1y}, must equal the indentation velocity, V.

The rate of internal energy dissipation is calculated by summing rates of energy dissipation for each discontinuous surface $(D_A)_n$. From the velocity and normal components of Table 1, the resulting strain rates are found from equation (4). The rate of energy dissipation is then calculated using equations (5) and (10). The rate of external work, W, is the product of the collapse pressure, P, the contact area, $t \cdot D$, and the velocity, V.

$$W = PtDV \tag{15}$$

Upper bounds for the indentation pressure can now be calculated by equating the rate of external work to the rate of internal energy dissipation. Hence,

$$P = [1/(tDv)] \sum_{n=1}^{8} (D_A)_n \tag{16}$$

After preliminary three-dimensional studies, it became evident that the optimum solutions were most sensitive to the block velocities and the out-of-plane surface normals and less sensitive to the in-plane geometry. Three-dimensional results were therefore calculated by holding these values constant at $\theta_1 = 0.85$, $\theta_2 = 1.05$, $\theta_3 = 0.20$, $\theta_4 = 0.45$ and $\theta_5 = 1.00$. The dependent angles $\theta_6 = 1.12$ and $\theta_7 = 0.57$, shown in Fig. 4, are thus also constant. Solutions may thus be obtained by numerically optimizing the velocity profile and geometry defined by the 13 variables, v_{1x}, v_{1z}, v_{2x}, v_{2y}, v_{2z}, v_{3x}, v_{3y}, v_{3z} β_1, β_2, β_3, β_4 and β_5.

Optimum upper-bound solutions are calculated using equation (16) for various aspect ratios and the results are shown in Fig. 7 (results are normalized with respect to uniaxial compressive strength). The optimum solutions show that, as should be expected, the out-of-plane surface normals and velocity components gradually decrease as the aspect ratio is

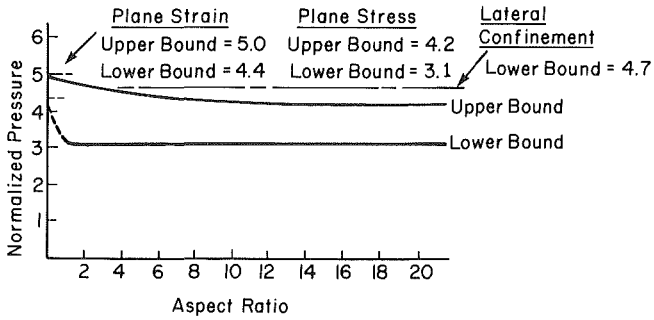

Fig. 7 Three-dimensional limit analysis solutions for normalized indentation pressure versus aspect ratio

decreased. In the limit as the aspect ratio approaches zero, the three-dimensional geometry and velocity fields reduce to the two-dimensional case shown in Fig. 2.

Also shown in Fig. 7 are the three-dimensional lower-bound solutions obtained by the method described by Karr (1988). For very low aspect ratios, but upper and lower-bound, three-dimensional results approach their respective plane strain, two-dimensional solutions (Karr et al., 1988). As the aspect ratio is increased, upper and lower-bound indentation pressures decrease with the upper-bound pressures decreasing more gradually. More complicated velocity field would be expected to improve the upper-bound solutions.

Plane Stress Solutions. For very high aspect ratios, the ice sheet is very thin relative to the indentor. For these conditions, the plane stress conditions may be assumed and two-dimensional solutions can be determined. The behavior of the three-dimensional solutions for large aspect ratios can then be compared to the plane stress solutions.

The lower-bound solution may be obtained by applying the yield function given by equation (7). For very thin ice sheets, the transverse stress components may be assumed to vanish; thus, $\sigma_{33} = \sigma_{23} = \sigma_{31} = 0$. Using the method described by Reinicke and Ralston (1977), the two-dimensional stress field shown in Fig. 8 was optimized. A lower bound for the normalized indentation pressure is found to be 3.12. Optimum values for the stress field were found for $p_1 = 0.30$, $p_2 = 0.25$, $\theta = 0.50$ and $\sigma = 0.45$. Note that the three-dimensional lower-bound solution approaches this value as the aspect ratio increases.

The upper-bound solution for the condition of plane stress is somewhat more complicated. This is because constraints on stress are first mapped to constraints on strain, and finally to constraints on surface normals and velocities. From equation (9), the stress constraints $\sigma_{33} = \sigma_{13} = \sigma_{32} = 0$ require

$$\epsilon_{23}' = 0 \qquad \epsilon_{31}' = 0$$

$$\epsilon_{33}' = \epsilon_{33}'(\epsilon_{11}', \epsilon_{22}', \epsilon_{12}') \tag{17}$$

The expression for ϵ_{33}' is quadratic. The expression for the rate of energy dissipation may then be written in the form

$$D = D(\epsilon_{11}', \epsilon_{22}', \epsilon_{12}') \tag{18}$$

We take the commonly used approach of starting with a two-dimensional velocity field as shown in Fig. 9. It is assumed at this point that ϵ_{33}' can be implicitly calculated to satisfy the plane strain requirement. The upper-bound solution for the indentation pressures can now be calculated by optimizing the velocity field of Fig. 9. An optimum solution for the normalized indentation pressure is found to be 3.51 with values for the velocity field of $\phi_1 = 0.0$, $\phi_2 = 0.1$, $\phi_3 = 0.3$, $\alpha_1 = 1.35$ and $\alpha_2 = 1.50$. Because we wish to compare this result to the three-dimensional results, the angles, θ_i, were held at the same constant values as mentioned previously.

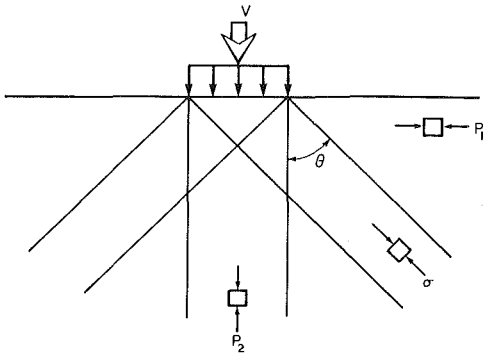

Fig. 8 Plane stress discontinuous stress field

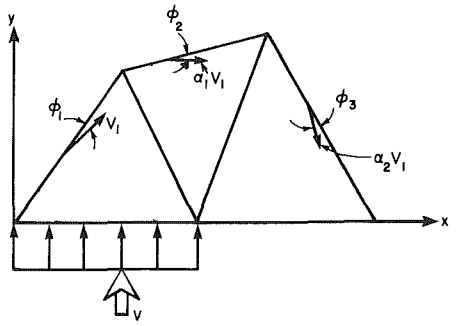

Fig. 9 Plane stress discontinuous velocity field

It is interesting to note that the three-dimensional, upper-bound solutions for large aspect ratios do not converge to the two-dimensional, plane-stress, upper-bound solution described in the foregoing. This is because of the use of flat, discontinuous velocity surfaces in the three-dimensional analyses. Applying the plane stress conditions results in strain rate constraints defined by equation (17). However, when three-dimensional surfaces of velocity discontinuity are used, the equivalent constraints are

$$\epsilon'_{23} = \frac{1}{2t}(n_2 v_3 + n_3 v_2) = 0$$

$$\epsilon'_{31} = \frac{1}{2t}(n_3 v_1 + n_1 v_3) = 0$$

$$\epsilon'_{33} = \frac{1}{t} n_3 v_3$$

$$= \epsilon'_{33}(n_1 v_1, n_2 v_2, n_2 v_1) \qquad (19)$$

Note that the three-dimensional velocity profiles (see Fig. 4) involve only discontinuous velocity surfaces, and thus the vertical strain-rate component ϵ'_{33} is proportional to $n_3 v_3$. For ϵ'_{33} to be nonzero, as is required by equation (17), n_3 and v_3 must also be nonzero. Upper-bound velocity profiles for plane-stress conditions therefore must include out-of-plane velocity and surface normal components. The area of the surfaces of velocity discontinuity will then depend on the angle of inclination of the surface.

This is in contrast to the two-dimensional fields in which the constraints on the strain rate component ϵ'_{33} are assumed to be satisfied, and thus the area of the surfaces of velocity discontinuities are assumed to be simply the product of the thickness times the length of the discontinuity. In the three-dimensional case, the angle of inclination (out of the plane of the sheet) must be determined. This affects the area of the surface of discontinuity, which in turn affects the rate of internal energy dissipation, and therefore results in a different (larger) indentation pressure.

V Conclusions

The upper and lower-bound solutions for the normalized indentation pressures for plane-strain conditions are very close: 4.68 ± 5 percent. As the aspect ratio is increased, the upper-bound indentation pressure approaches a limiting value of approximately 4.20, while the lower-bound plane stress solution is determined to be 3.12. Thus, the plane stress indentation pressure is 3.65 ± 15 percent.

A significant feature of the plane stress solution is that the ice sheet indentation pressure is below the collapse stress for conditions in which the ice is fully confined in the lateral direction. For very thick ice there is enough confinement (both laterally and vertically) to require indentation pressures well above the uniaxial compressive strength, and also above the laterally confined strength. For thin ice, however, the vertical confinement vanishes and the lateral confinement is reduced such that indentation occurs below the laterally confined strength. Both the upper and lower-bound solutions indicate that the indentation pressures decrease to a constant limiting value as the aspect ratio is increased.

Some improvement could be achieved by increasing the complexity of the rigid block velocity profiles. There is also some inherent overprediction of the upper bounds using the flat discontinuous surfaces. This is easily demonstrated by examining the uniaxial compression case. The lower-bound solution is exact with a normalized compression strength of 1.0. Using the velocity profile shown in Fig. 10 as an upper-bound velocity field results in a normalized compressive strength of 1.24. Thus, the upper bound for this very simple case is 24 percent above the exact value.

This may explain why the upper-bound indentation pressure for high aspect ratios is nearly 35 percent higher than the lower bound. This also suggests that the plane stress upper bounds may overestimate the actual plastic indentation pressures. We note also that the plane stress conditions imply either: 1) relatively thin ice for which other failure mechanism would be more critical, or 2) very wide indentors for which perfect contact is nearly impossible. Both theoretical and experimental studies suggest that plastic limit analysis is most appropriate for low aspect ratios. First of all, relatively thick ice (low aspect ratios) is less susceptible to other failure mechanisms, such as out-of-plane bending or buckling. Additionally, the stress states are more predominantly compressive for lower aspect ratios, and thus plastic flow is generally more likely than brittle deformation. Also, experimental results for low aspect ratios show measured stresses during ice/structure interactions in the range of stresses predicted by limit analysis.

It has long been recognized that the aspect ratio is an important parameter for determining ice/structure interaction forces. This is perhaps more obvious if one considers different

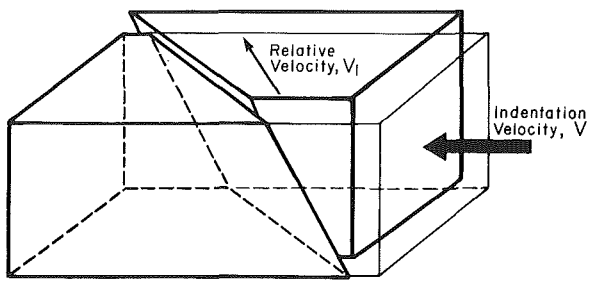

Fig. 10 Upper-bound velocity profile for uniaxial compression

failure mechanisms, such as ice sheet fracture, bending failure or buckling modes. The present study has established the importance of the aspect ratio even when only one failure mechanism is addressed: plastic collapse. Both the state of stress within the ice sheet and the plastic collapse mechanisms are three dimensional. This study highlights the importance of the three-dimensional nature of the ice sheet indentation problem.

Acknowledgments

This material is based upon work supported by the National Science Foundation under Grant No. CEE 8404687. Additional support provided by the Sea Grant College Program at MIT is gratefully acknowledged.

References

Bohon, W. M., and J. S. Weingarten, 1985, "The Calculation of Ice Forces on Arctic Structures," *Proceedings of the ASCE Arctic 1985 Congress.*

Chen, W. F., 1975, *Limit Analysis and Soil Plasticity*, Elsevier Press, Amsterdam.

Croasdale, K. R., Morgenstern, N. R., and Nuttall, J. B., 1977, "Indentation Tests to Investigate Ice Pressures on Vertical Piers," *Journal of Glaciology*, Vol. 19, No. 81, pp. 301–312.

Drucker, D. C., and Prager, W., 1952, "Soil Mechanics and Plastic Analysis or Limit Design," *Quarterly Journal of Applied Mathematics*, X, pp. 157–165.

Feng, W. W., and Yang, W. H., 1984, "General and Specific Quadratic Yield Functions," *Compos. Technology Review*, Vol. 6, p. 19.

Hausler, F. V., 1981, "Multiaxial Compressive Strength Tests on Saline Ice with Brush-Type Loading Plates," *IAHR International Symposium on Ice*, Vol. II, pp. 526–536.

Karr, D. G., 1988, "Three-Dimensional Analysis of Ice Sheet Indentation: Lower Bound Solutions," ASME JOURNAL OF OFFSHORE MECHANICS AND ARCTIC ENGINEERING, Vol. 110, pp. 81–86.

Karr, D. G., Law, F. P., HooFatt, M., and Cox, G. F. N., 1989, "Asymptotic and Quadratic Failure Criteria for Anisotropic Materials," *International Journal of Plasticity.*

Michel, B., and Toussaint, N., 1977, "Mechanisms and Theory of Indentation of Ice Plates," *Journal of Glaciology*, Vol. 19, No. 81, pp. 285–299.

Olszak, W., and Urbanowski, W., 1956, "The Plastic Potential and the Generalized Distortion Energy in the Theory of Non-Homogeneous Anisotropic Elastic-Plastic Bodies," *Arch. Mech. Stosowanej*, Vol. 8, pp. 671–693.

Palmer, A. C., et al., 1983, "Fracture and Its Role in Determining Ice Forces on Offshore Structures," *Annals of Glaciology*, Vol. 4, pp. 216–221.

Ralston, T. D., 1978, "An Analysis of Ice Sheet Indentation," *4th International Symposium on Ice Problems*, IAHR, Lulea, Sweden.

Reinicke, K. M., and Ralston, T. C., 1977, "Plastic Limit Analysis with an Anisotropic, Parabolic Yield Function," *International Journal of Rock Mechanics, Mining Sciences and Geomechanics Abstracts*, Vol. 14, pp. 147–154.

Reinicke, K. M., and Remer, R., 1978, "A Procedure for the Determination of Ice Forces: Illustrated for Polycrystalline Ice," *Proceedings of the IAHR Symposium on Ice Problems*, Part 1, Lulea, Sweden, pp. 217–238.

Sanderson, T. J. O., 1987, "A Pressure-Area Curve for Ice," *Proceedings of the 8th International Symposium on Ice*, IAHR, Iowa City, Iowa.

Timco, G. W., 1987, "Indentation and Penetration of Edge-Loaded Freshwater Ice Sheets in the Brittle Range," ASME JOURNAL OF OFFSHORE MECHANICS AND ARCTIC ENGINEERING, Vol. 109, pp. 287–294.

Tsai, S. W., and Wu, E. M., 1971, "A General Theory of Strength for Anisotropic Materials," *Journal of Composite Materials*, Vol. 5, pp. 58–80.

Wierzbicki, T., and Karr, D. G., 1987, "Structural Imperfections and Interactive Failure of Edge-Loaded Ice Sheets," *Proceedings of the 9th International Conference on Port and Ocean Engineering under Arctic Conditions*, Fairbanks, Alaska.